FINITE ELEMENT ANALYSIS OF THE ECT TEST ON MODE III INTERLAMINAR FRACTURE OF CARBON-EPOXY COMPOSITE LAMINATES

M.F.S.F. de MOURA*, M.A.L. SILVA, A. B. de MORAIS***, J.J.L. MORAIS****

*** University of Porto, Faculty of Engineering, Department of Mechanical Engineering and Industrial Management, R. Dr. Roberto Frias, 4200-465 Porto**
mfmoura@fe.up.pt
**** CETAV/UTAD, Department of Mechanical Engineering, Quinta de Prados, 5000-911, Vila Real.**
mlsilva@utad.pt, jmorais@utad.pt
***** University of Aveiro, Department of Mechanical Engineering, Campus Santiago, 3810-193 Aveiro**
abm@mec.ua.pt

Abstract. In this work a parametric study of the Edge Crack Torsion (ECT) specimen was performed in order to maximize the mode III component (G_{III}) of the strain energy release rate for carbon-epoxy laminates.
A three-dimensional finite element analysis of the ECT test was conducted considering a $[90/0/(+45/-45)_2/(-45/+45)_2/0/90]_S$ lay-up. The main objective was to define an adequate geometry to obtain an almost pure mode III at crack front. The geometrical parameters studied were specimen dimensions, distance between pins and size of the initial crack.
The numerical results demonstrated that the ratio between the specimen length and the initial crack length had a significant effect on the strain energy release rate distributions. In almost all of the tested configurations, a mode II component occurred near the edges but it did not interfere significantly with the dominant mode III state.

1. INTRODUCTION

Interlaminar fracture in composite materials is a very complicated phenomenon, often accompanied by intraply micro-cracking. The fracture phenomenon can be characterized in three loading modes: mode I, mode II and mode III. The test techniques for delamination on mode I have been well established [1,2]. Mode II delamination has also received significant attention in the research community [3-5].

On the other hand, mode III fracture has been less studied due to the experimental difficulties in introducing pure mode III loading at the crack front. A mode III test is needed for complete characterization of the three fracture modes. Several testing methods have been proposed to evaluate the mode III critical energy release rate (G_{IIIc}). Donaldson [6] proposed the Split Cantilever Beam (SCB) specimen. However, finite element analysis and scanning electron microscopic fractographs of the SCB specimens showed that significant mode II exist [7,8]. Cicci et al. [8] developed a new experimental technique for the SCB test, in order to minimize the mode II component. This technique consists on a reformulation of the loading system. In spite of the decrease of the mode II component, it is not sufficient to affirm that this test is adequate to obtain the mode III fracture properties. Becht et al. [9] used a Crack Rail Shear (CRS) test for mode III interlaminar fracture toughness characterization. The CRS specimen with double cracks may have difficulties in growing both cracks simultaneously; although a modified single crack CRS could solve this problem. However, both CRS configurations have relatively low compliance which makes it difficult to obtain fracture toughness by the compliance calibration method [10]. Farshad et al. [11] proposed the Anti-Clastic Plate Bending (ACPB) to obtain the G_{IIIc}. The ACPB test can be produced by applying two pairs of point loads normal to the plate at two diagonally opposite corners or a pair of twisting moments acting along two opposite edges.

A new mode III test, the Edge Crack Torsion (ECT) method, has been evaluated experimentally and analytically as a candidate standard mode III fracture toughness test for laminated composites [12,13]. It was proposed by Lee [14], who used a $[90/(+45/-45)_n/(-45/45)_n/90]_s$ laminate with a mid-plane free

edge delamination. Zhao et al. [15] conducted a three-dimensional finite element analysis on a $[90/(+45/-45)_n/(-45/45)_n/90]_s$ class of laminated composite. From this study the authors concluded that the delamination grows in pure mode III in the middle region of the specimen and that friction between crack faces has a negligible effect on measurements.

The main objective was to define an adequate geometry to obtain an almost pure mode III condition. For this, a three-dimensional finite element analysis of the ECT test was performed considering a $[90/0/(+45/-45)_2/(-45/+45)_2/0/90]_S$ lay-up. The main objective was to define an adequate geometry to obtain an almost pure mode III distribution of strain energy release rate, a long the crack tip. The geometrical parameters studied were the specimen dimensions, the distance between pins and the influence of the initial crack length.

2. ECT SPECIMEN ANALYSIS

The original ECT specimen geometry is represented in figure 1. The dimensions used for the ECT specimen were: L=90 mm, L'=76 mm, B=38 mm, W=32 mm, a_0=13 mm and t=4.5 mm. The ECT test consists of a load frame where the specimen is positioned between three support pins, and loaded via a fourth pin, as illustrated in figure 1. The specimen stacking sequence used for the carbon-epoxy composite laminates was $[90/0/(+45/-45)_n/(-45/45)_n/0/90]_s$, with n=2. The orthotropic ply properties used for the carbon-epoxy material are presented in table 1.

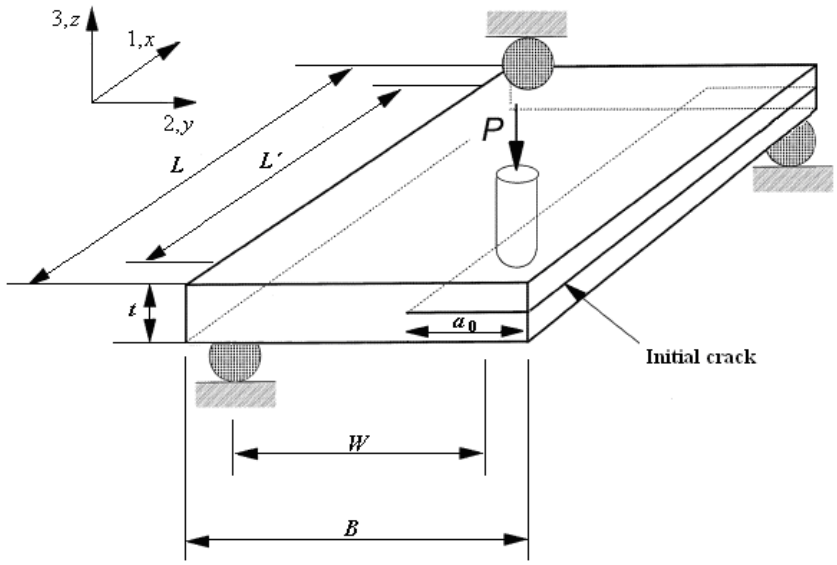

Fig. 1 – Geometry of the ECT specimen.

E_1 (GPa)	E_2 (GPa)	E_3 (GPa)	υ_{12}	υ_{13}	υ_{23}	G_{12} (GPa)	G_{13} (GPa)	G_{23} (GPa)
110	8	8	0.35	0. 35	0.38	3.2	3.2	2.8

Table 1 – Material properties of carbon-epoxy laminate [16]

Due to the nature of out-of-plane deformation for the ECT specimen configuration, a three-dimensional finite element model was necessary. This numerical model was constructed within the software ABAQUS® using three-dimensional 8-node brick elements. The strain energy release rates distribution at crack tip were obtained using 8-node interface finite elements, previously developed [17,18]. The number of brick and interface finite elements was varied in each model geometry in order to keep, in

all analyses, the same size of the elements. In the region of the initial crack contact conditions were imposed to prevent interpenetration of the cracked parts. The interface finite elements were placed at the mid-plane of the uncracked region ($t/2$). The supports and actuator pins were simulated as rigid bodies (Figure 2).

The profiles of the strain energy release rates at crack tip of the ECT specimen were obtained by an adaptation of the Virtual Crack Closure Technique (VCCT). In this case, (see figure 3) stresses and relative displacements at the nodes of the interface elements are used in order to obtain,

$$\begin{aligned} G_{\mathrm{I}} &= \frac{\sigma_{j3}(w_{k\,\mathrm{t}} - w_{k\,\mathrm{b}})}{2} \\ G_{\mathrm{II}} &= \frac{\tau_{j31}(u_{k\,\mathrm{t}} - u_{k\,\mathrm{t}})}{2} \\ G_{\mathrm{III}} &= \frac{\tau_{j32}(v_{k\,\mathrm{t}} - v_{k\,\mathrm{t}})}{2} \end{aligned} \tag{1}$$

where σ_{j3}, τ_{j31} and τ_{j32} denote the nodal stresses at the delamination front. The corresponding displacements behind the delamination at the top face (node kt) are represented by $u_{k\mathrm{t}}$, $v_{k\mathrm{t}}$ and $w_{k\mathrm{t}}$, and at the lower face (node kb) are designated by $u_{k\mathrm{b}}$, $v_{k\mathrm{b}}$ and $w_{k\mathrm{b}}$ as shown in figure 3.

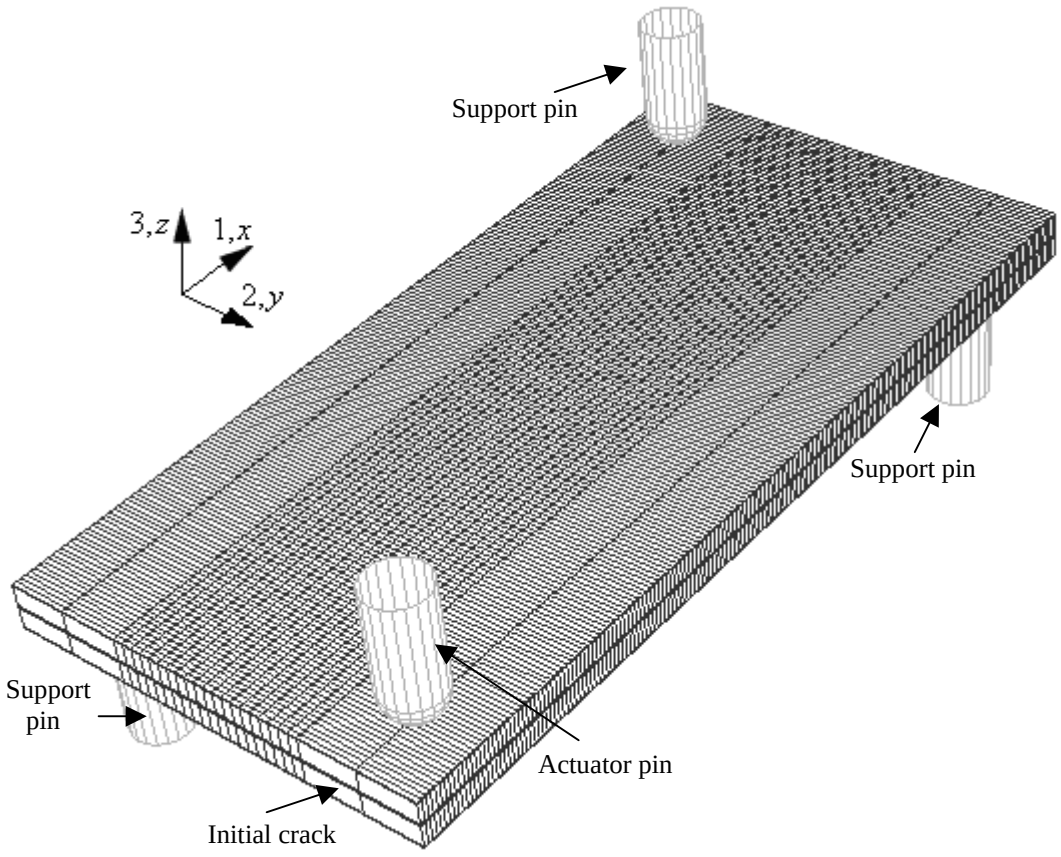

Fig. 2 – Element finite mesh.

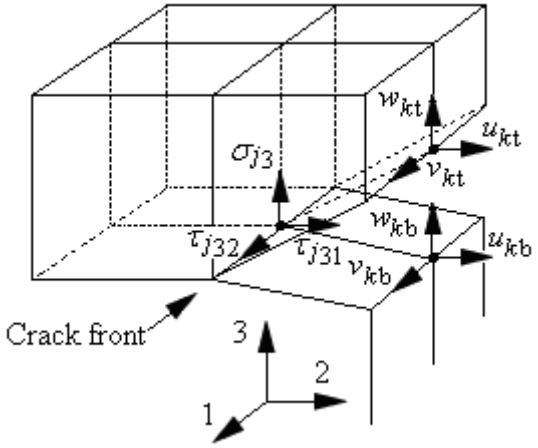

Fig. 3 – Scheme of the local nodes used for the VCCT.

3. PARAMETRIC STUDY

This section is divided in three analyses: in the first two, a geometrical improvement in the *x* and *y* directions were performed; finally, the influence of the initial crack length (a_0) on the strain energy release rates distributions at the crack front is also analysed. The selection of the best geometry for the ECT specimen is based on two criteria: in the first one, all configurations where the strain energy released rate in mode II (G_{II}) is higher than 3% will be excluded, and in the second criterion the configuration that presented the best compromise between the maximization of G_{III} and specimen material cost will be selected.

3.1. *x*-direction geometry

In this study, three values for the distance between the edge of the specimen and the supports (*L*-*L´*) (see figure 1) were evaluated: 7, 16, 25 mm, corresponding to the configurations A*i*, B*i* and C*i*, respectively. For each value of *L*-*L´*, a variation, different values of *L´* considered were: *L´*= 38, 76, 91 and 106 mm that correspond to *i*=1, 2, 3, 4, respectively.

Table 1 lists a comparison between the average values of the three components of the strain energy release rate (G_I, G_{II}, G_{III}) and the total strain energy release rate (G_{TOTAL}). From this table it can be concluded that, for all configurations, the energy release rate in mode I (G_I) is negligible. From the above criteria the configurations A1, A2, A3, A4, B1 and C1 were eliminated. For B*i* configurations, G_{II} was always less than 3% of G_{TOTAL}. However, relative to B2, the manufacturing of the B4 and B3 configurations involve an increase of material consumption of 39.74% and 19.74%, respectively, but they only reduce slightly the presence of mode II. The same situation was observed when the C2, C3 and C4 configurations were compared. Finally, for the best configurations selected, when the C2 is used instead of B2, the volume of material increases 16.7% and the presence of mode II only decrease 0.17%. Consequently, it can be concluded that the best configuration is B2. This test configuration has the distances: *L´*=76 mm and *L*-*L´*= 16 mm.

Configuration test	G_I (N/mm)	G_{II} (N/mm)	G_{III} (N/mm)	G_{TOTAL} (N/mm)	Presence of Mode I (%)	Presence of Mode II (%)	Presence of Mode III (%)
***L-L´* = 7 mm**							
A1	3,64E-08	5,92E-05	7,39E-04	7,99E-04	0,0	7,4	92,6
A2	1,16E-09	2,57E-06	6,05E-05	6,31E-05	0,0	4,1	95,9
A3	5,84E-10	1,60E-06	4,42E-05	4,58E-05	0,0	3,5	96,5
A4	4,62E-10	1,05E-06	3,37E-05	3,48E-05	0,0	3,1	96,9
***L-L´* = 16 mm**							
B1	4,41E-09	7,62E-06	1,38E-04	1,46E-04	0,0	5,2	94,8
B2	6,81E-10	1,42E-06	5,10E-05	5,24E-05	0,0	2,7	97,3
B3	4,25E-10	8,91E-07	3,81E-05	3,90E-05	0,0	2,3	97,7
B4	2,79E-10	5,96E-07	2,96E-05	3,02E-05	0,0	1,9	98,1
***L-L´* = 25 mm**							
C1	3,04E-09	5,77E-06	1,12E-04	1,18E-04	0,0	4,9	95,1
C2	5,08E-10	1,15E-06	4,42E-05	4,53E-05	0,0	2,5	97,5
C3	3,31E-10	7,35E-07	3,36E-05	3,43E-05	0,0	2,1	97,9
C4	2,21E-10	4,99E-07	2,64E-05	2,69E-05	0,0	1,9	98,1

Table 2 – Comparison between the average values of G_I, G_{II} and G_{III} and the total energy release rate G_{TOTAL} for the configurations studied.

3.2. *y*-direction geometry

The parametric analysis of the ECT specimen in the *y* -direction was divided in two steps. The first step corresponds to the variation of the distance between the edge of the specimen and the pins (*B*-*W*), keeping the distance between the pins constant (*W*=32 mm). The different values of *B*-*W* considered were: 3, 6, 9 mm, which correspond to the D1, D2 and D3 configurations, respectively. From this analysis the distance *B*-*W*, that maximizes the G_{III} at crack tip was obtained. The second step consists in studying the influence of *W* on *G*-distributions keeping *B*-*W* constant. The different values of *W* used in this numerical study were: 32, 47, 62 mm, which correspond to the E1, E2 and E3 configurations, respectively.

As can be seen in table 3, the presence of G_I at the crack tip can be considered negligible for all configurations. All D*i* configurations satisfy the first selection criterion. However, the D1 configuration presents an important G_{II} component when compared with the D2 and D3 configurations. Consequently, this configuration was eliminated. The manufacturing of D3 instead of D2 configuration leads to a 13.6% increase of material consumption, but only induces a reduction of 0.5% on G_{II}/G ratio. Therefore, it can be concluded that D2 configuration is the best one. This configuration corresponds to the distance *B*-*W* equal to 6 mm. As mentioned above the distance *B*-*W* is an inputted parameter on the second step of the geometrical study. From the results obtained in the second step (Table 2), it can be concluded that only the E1 configuration respect the first criterion of selection. Figure 4 shows the chosen geometry. This geometry represents the best compromise between the presence of G_{III} at crack tip and the material consumption for manufacturing the experimental specimens.

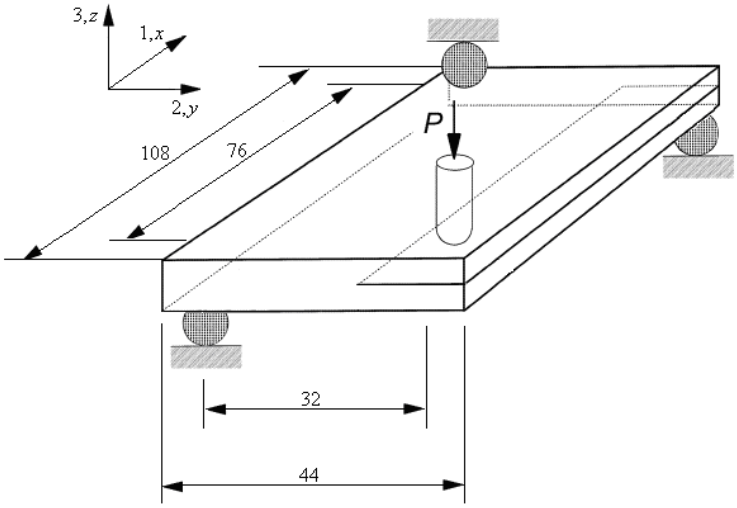

Fig. 4 – The ECT specimen geometry selected.

Configuration test	G_I (N/mm)	G_{II} (N/mm)	G_{III} (N/mm)	G_{TOTAL} (N/mm)	Presence of Mode I (%)	Presence of Mode II (%)	Presence of Mode III (%)
D1	5,10E-05	6,81E-10	1,42E-06	5,24E-05	0,0	2,7	97,3
D2	5,18E-05	8,82E-10	4,68E-07	5,23E-05	0,0	0,9	99,1
D3	5,19E-05	5,20E-09	2,14E-07	5,22E-05	0,1	0,4	99,5
E1	8,82E-10	4,68E-07	5,18E-05	5,23E-05	0,0	0,9	99,1
E2	4,28E-10	9,43E-07	2,87E-05	2,96E-05	0,0	3,2	96,8
E3	2,39E-10	1,19E-06	1,87E-05	1,99E-05	0,0	6,0	94,0

Table 3 – Comparison between the average values of G_I, G_{II} and G_{III} and the total energy release rate G_{TOTAL} for the different *y*-direction configurations.

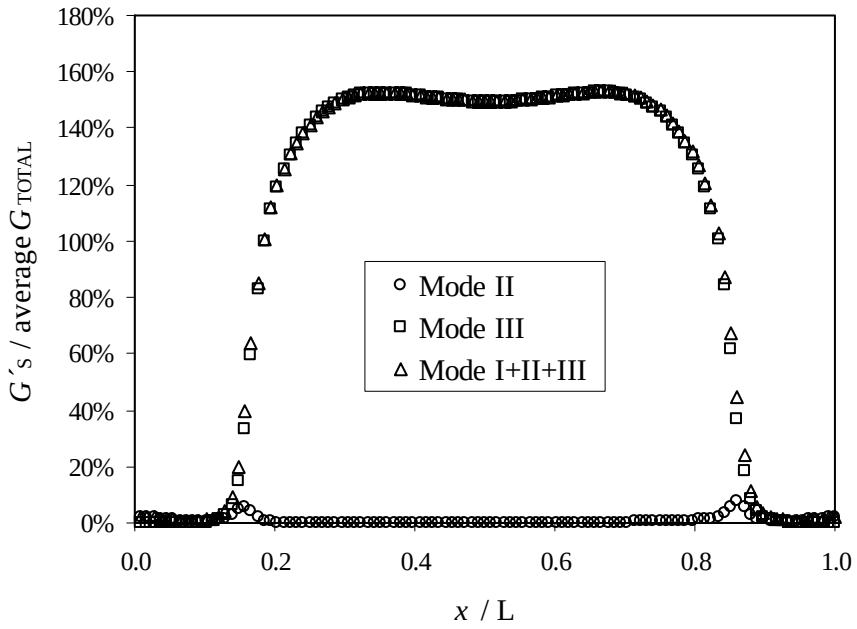

Fig. 5 – Energy release rates distributions G'_S (G_{II}, G_{III} and G_{TOTAL}), normalised by the average value of G_{TOTAL}, for the selected specimen geometry.

It can be observed in figure 5 that G_{II} is negligible at the middle of the specimen, presenting small peaks at the pins vicinity. In fact, for the selected geometry, the distributions of G_{III} and G_{TOTAL} are practically identical, showing an almost pure mode III is achieved: G_{III} represents 99.1% of G_{TOTAL}.

3.3. Influence of the initial crack length (a_0)

The influence of the initial crack (a_0) on the strain energy release rates profiles was also performed. In this study different relations a_0/B, between the a_0 and the width of the specimen (B) were considered: 0.2, 0.3, 0.4, 0.5 and 0.6, which are designated by F1, F2, F3, F4 and F5 configurations, respectively.

The mode I strain energy release rate (G_I) along the edge delamination front is negligible for all configurations studied. The presence of mode II energy release rate (G_{II}) increases with the a_0/B ratio (table 4). Hence, it can be concluded that the best configuration is F1. The distributions of G_{II}, G_{III} and G_{TOTAL} for the F1 configuration with the selected geometry in the x and y-directions can be observed in figure 6.

Configuration test	G_I (N/mm)	G_{II} (N/mm)	G_{III} (N/mm)	G_{TOTAL} (N/mm)	Presence of Mode I (%)	Presence of Mode II (%)	Presence of Mode III (%)
F1	8,82E-10	4,68E-07	5,18E-05	5,23E-05	0,0	0,9	99,1
F2	8,96E-10	2,50E-06	4,93E-05	5,18E-05	0,0	4,8	95,2
F3	7,08E-10	3,80E-06	4,71E-05	5,09E-05	0,0	7,5	92,5
F4	5,31E-10	4,32E-06	4,51E-05	4,94E-05	0,0	8,7	91,3
F5	4,29E-10	3,80E-06	4,31E-05	4,69E-05	0,0	8,1	91,9

Table 4 – Comparison between the average values of G_I, G_{II}, G_{III} and G_{TOTAL} for different a_0/B ratios.

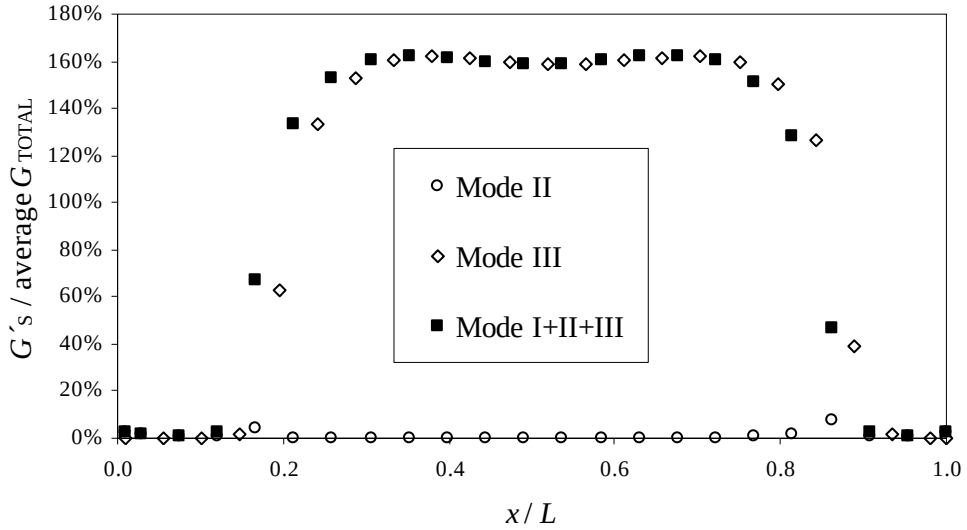

Fig. 6 – Energy release rates distributions (G_{II}, G_{III} and G_{TOTAL}), normalised by the average value of G_{TOTAL}, for the relation a_0/B=0.2.

4. CONCLUSIONS

In this work a three-dimensional finite element model was constructed, in order to select an ECT specimen geometry with an almost pure mode III at crack front. The selection procedure was based on the energy release rate profiles along of the crack tip. The strain energy release rate components (G_I, G_{II} and G_{III}) were obtained by an adaptation of the Virtual Crack Closure Technique (VCCT). The numerical model was based on three-dimensional 8-node brick and 8-nodes interface finite elements previously developed.

The geometry selection for the ECT specimen was based on two criteria: in the first one, all configurations for which the G_{II}/G_{TOTAL} ratio was higher than 3% were excluded; in the second one the configuration that presented the better compromise between the maximization of G_{III} and specimen material costs were selected. The parametric study was divided in three analyses: in the first two, the ideal geometry in the *x* and *y* directions were defined; thirdly, the influence of the initial crack length (a_0) on the energy release rate distributions was evaluated.

The selected ECT configuration has G_{III}/G_{TOTAL} = 99.1%, and therefore is considered adequate to measure G_{IIIc} of carbon-epoxy composite laminates.

5. ACKNOWLEDGMENTS

The authors thankful the Portuguese Foundation for Science and Technology (FCT, research project POCTI/EME/45573/2002) for supporting the work here present.

REFERENCES

[1] Davidson, B.D., Kruger, R., Konig, M., "Effects of stacking sequence on energy release rate distributions in multidirectional DCB and ENF specimens", Eng. Fract. Mech., 55, 557-569 (1996).

[2] Hojo, M., Kageyama, K., Tanaka, K., "Prestandardization study on mode I interlaminar fracture toughness test for CFRP in japan", Composites, 26, 243-255 (1995).

[3] Silva, M.A.L., de Moura, M.F.S.F. and Morais, J.J.L., "Numerical analysis of the ENF test for mode II wood fracture" *in press* on Composites Part A, 2005.

[4] Silva, M.A.L., et al, "Numerical analysis of the ENF test on the mode II fracture of wood", In: Proceedings of the III conference of ESWM 2004, Vila Real, pp. 77-84.

[5] Silva, M.A.L., et al, "Análise por elementos finitos do ensaio ENF (End Notched Flexure) para a determinação das propriedades de fractura da madeira, Pinus Pinaster.Ait.", In: Proceedings of Congreso de Métodos Numéricos en Ingeniéria 2005, Granada, pp. 279.

[6] S.L. Donaldson, "Mode III interlaminar fracture characterization of composite materials", Composite Science and Technology, 32, 225-249 (1988).

[7] Martin, R.H., "Evaluation of the split cantilever beam for mode III interlaminar delamination testing, Composite Materials: Fatigue and Fracture (third volume), ASTM STP 1110, O´Brien, T.K., Ed., American Society for Testing and Materials.

[8] Cicci, D., Sharif, F., Kortschot, M.T., "Data reduction for the split cantilever beam mode III delamination test", In: Proccedings of ICCM-10 1995, Canada, pp. 189-196.

[9] Becht, G., Gillespie, J.W., Jr., "Design and analysis of the cracked rail shear specimen for mode III interlaminar fracture" Composite Science and Technology, 31, 143-157 (1988).

[10] Barry, J.P., "Determination of fracture energies by the cleavage technique", Journal of Applied Physics, 34, 62-68 (1963).

[11] Farshad, M., Flueler, P., "Investigation of mode III fracture toughness using an anti-clastic plate bending method", Eng. Fract. Mech., 60, 597-603 (1998).

[12] Li, J., O´Brien, T.K., "Simplified data reduction methods for the ECT test for mode III interlaminar fracture toughness", Journal of Composites Technology and Research, 18, 96-101 (1996).

[13] Li, J., O´Brien, T.K., "Analytical investigation of the hygrothermal effects and parametric study of the edge crack torsion (ECT) mode III test lay-ups", Composite Materials: Fatigue and Fracture, ASTM STP 1285, 1997.

[14] S.M. Lee, "An edge crack torsion method for mode III delamination fracture testing", Composite Technology Research, 15(3), 193-201 (1993).

[15] Zhao, D., Wang, Y., "Mode III fracture behaviour of laminated composite with edge crack in torsion" Theoretical and Applied Fracture Mechanics, 29, 109-123 (1998).

[16] de Moura, M.F.S.F., et al, "Análise numérica e experimental do ensaio ECT (Edge Crack Torsion) em materiais compósitos", In: Proceedings of Congreso de Métodos Numéricos en Ingeniéria 2005, Granada, pp. ??.

[17] Gonçalves, J.P.M., de Moura, M.F.S.F., Castro, P.M.S.T., Marques, A.T., "Interface element including point-to-surface constraints for three dimensional problems with damage propagation", Engineering Computations, 17, 28-47 (2000).

[18] de Moura, M.F.S.F., Gonçalves, J.P.M., Marques, A.T., Castro, P.M.S.T., "Modeling compression failure after low velocity impact on laminated composites using interface elements", Journal of Composite Materials, 31, 1462-1479 (1997).